

The FLUKA nuclear cascade model applied to neutrino interactions

G. Battistoni^a, A. Ferrari^{b*}, A. Rubbia^c, P.R. Sala^{cc†}

^aINFN, Sezione di Milano, Via Celoria 16, 20133 Milan, Italy

^bCERN, CH-1211 GENÈVE 23, Switzerland

^cInstitut für Teilchenphysik, ETHZ, CH-8093 Zürich, Switzerland

The NUX-FLUKA ν -nucleus event generator is briefly described with examples of the predicted effect of the nuclear environment on kinematical variables.

1. INTRODUCTION

Nuclear effects in neutrino interactions are one of the main topics of this workshop. The approach we present here is the coupling of a “free” ν -nucleon event generator (NUX) with the well established and tested nuclear “environment” of the Monte Carlo FLUKA code. In this way, both Initial State and Final State effects are taken into account, and their impact on the reaction kinematics can be disentangled. This will be illustrated with several examples in the following sections, where kinematic quantities will be presented in the:

- *Initial State*: particles as they are produced inside the nucleus by the primary ν -nucleon interaction
- *Final State* : particles emitted in the reaction, all nuclear effects included
- *No reinteractions*: particles emitted in the reaction, when reinteraction processes are inhibited. These differ from the Initial State configuration due to the effect of nuclear potentials.

The examples shown here refer mainly to ν_μ interactions in Oxygen and Iron, in the 0.5 to 10 GeV range. However, NUX-FLUKA is capable to handle interactions on any target material/compound, for energies up to 10 TeV and for all neutrino flavors.

*On leave of absence from INFN Milan

†On leave of absence from INFN Milan

We refer to the literature [1,2] for general descriptions of the two codes. Here we give some details about the features relevant to ν interactions.

2. PEANUT

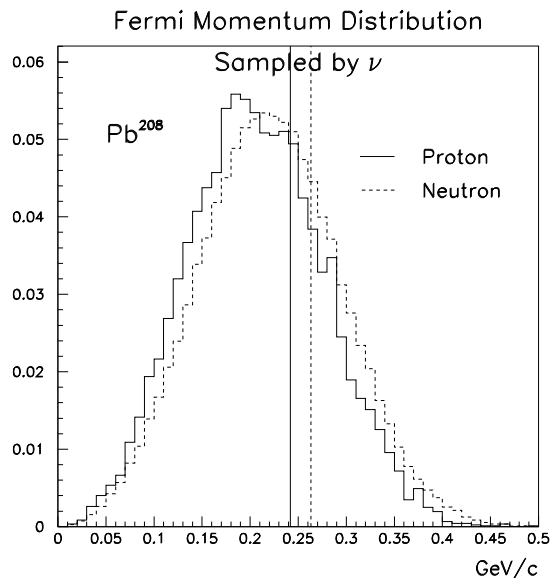


Figure 1. Fermi momentum distribution as sampled by ν_μ in ^{208}Pb . Proton and neutron distributions are shown together with un-smearred maximum from central density.

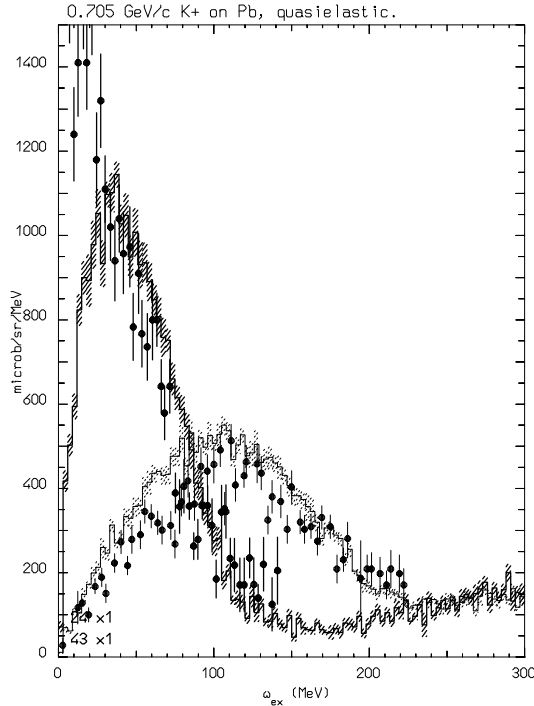


Figure 2. ($K^+, K^{+'}$) on Pb vs residual excitation, 705 MeV/c, at 24° and 43° . Histo:FLUKA, dots:data[13]. Elastic scattering is not included in the calculations. On free nucleon the recoil recoil energy is 43 MeV at 24° , 117 MeV at 43° .

The intermediate energy hadronic model of FLUKA is called PEANUT. Presently, PEANUT handles interactions of nucleons, pions, kaons, and γ rays from about 4 GeV down to reaction threshold (or 20 MeV for neutrons). The reaction mechanism is modelled in PEANUT by explicit (generalized) intranuclear cascade (GINC) smoothly joined to statistical (exciton) preequilibrium emission [3,4].

At the end of the GINC and exciton chain, the evaporation of nucleons and light fragments (α , d, ^3H , ^3He) is performed, following the Weisskopf [5] treatment. Competition of fission with evaporation has been implemented, again within a statistical approach. Since the statistical evaporation

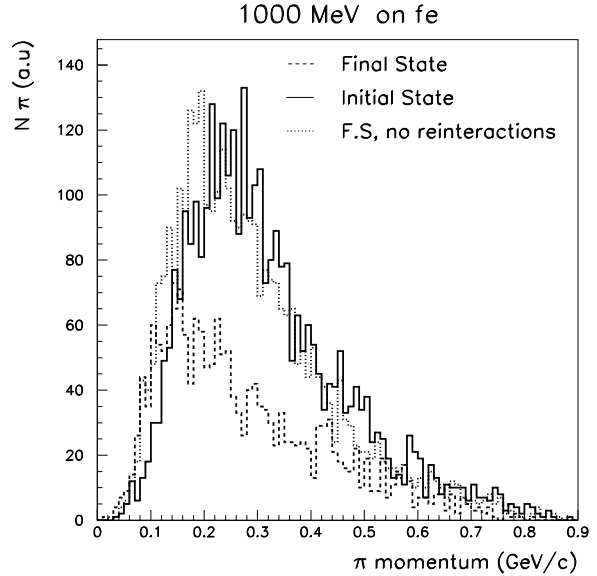


Figure 3. Charged pion spectra after 1 GeV ν_μ interaction on Iron.

model becomes less sound in light nuclei, the so called Fermi Break-up model [6,7] is used instead. The excited nucleus is supposed to disassemble just in one step into two or more fragments, with branching given by plain phase space considerations, corrected for Coulomb barriers when applicable.

The excitation energy still remaining after (multiple) evaporation is dissipated via emission of γ rays [8].

2.1. GINC GENERALITIES

The GINC proceeds through hadron multiple collisions in a cold Fermi gas. The hadron-nucleon cross sections used in the calculations are the free ones modified by Pauli blocking, except for pions and negative kaons that deserve a special treatment. The Fermi motion is taken into account, both to compute the interaction cross section, and to produce the final state particles.

Secondaries are treated exactly like primary particles, with the only difference that they start their trajectory already inside the nucleus. Primary and secondary particles are transported according to their nuclear mean field and to the

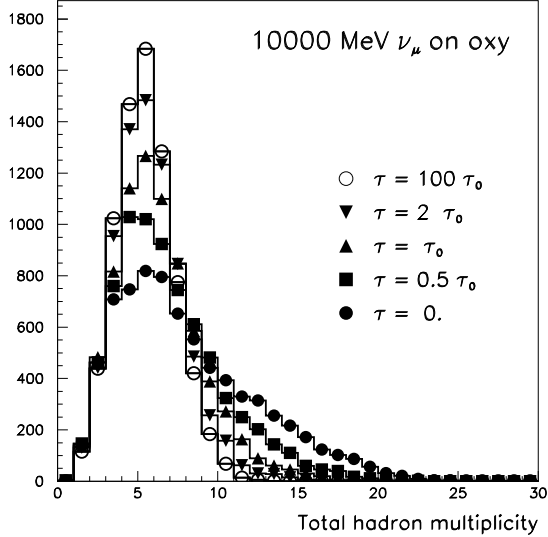


Figure 4. Effect of different formation time (τ) values on the total hadron multiplicity in 10 GeV ν_μ CC interactions on Oxygen.

Coulomb potential. All particles are transported along classical trajectories, nevertheless a few relevant quantum effects are included.

Binding Energies (B_{en}) are obtained from mass tables, depending on particle type and on the actual composite nucleus, which may differ from the initial one in case of multiple particle emission. Relativistic kinematics is applied, with accurate conservation of energy and momentum, and with inclusion of the recoil energy and momentum of the residual nucleus.

2.2. Nuclear geometry

In both stages, INC and exciton, the nucleus is modelled as a sphere with density given by a symmetrized Woods-Saxon [9] shape for $A > 16$,

$$\rho(r) = \rho_0 \frac{\sinh(R_0/a)}{\cosh(r/a) + \cosh(R_0/a)} \approx \frac{\bar{\rho}_0}{1 + \exp \frac{r-R_0}{a}} \quad (1)$$

and by a harmonic oscillator shell model for light isotopes (see [10]). Proton and neutron densities are generally different, according again to

shell model ones for $A < 16$, and to the droplet model [11,12] for heavier nuclei.

2.3. Fermi motion and Nuclear Potential

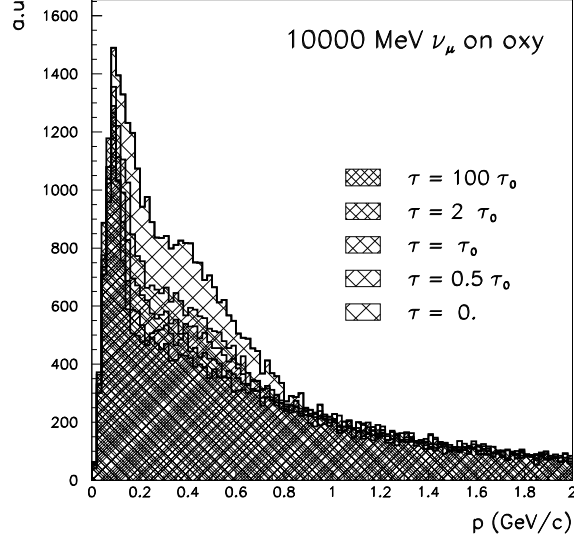


Figure 5. Effect of different formation time (τ) values on the charged hadron spectra in 10 GeV ν_μ CC interactions on Oxygen.

A standard position dependent Fermi momentum distribution is implemented in PEANUT :

$$\frac{dN}{dk} = \frac{|k|^2}{2\pi^2} \quad (2)$$

for k up to a local Fermi momentum $k_F(r)$ given by

$$k_F^{p,n}(r) = (3\pi^2 \rho^{p,n}(r))^{\frac{1}{3}} \quad (3)$$

where $\rho^{p,n}$ is the neutron or proton density as defined in the previous paragraph. Fermi momentum is smeared according to the uncertainty principle assuming a position uncertainty $= \sqrt{2} \text{ fm}$. An example of the resulting distribution is shown in fig.1.

The potential depth felt by nucleons at any radius r is given by the Fermi energy plus the relevant binding energy.

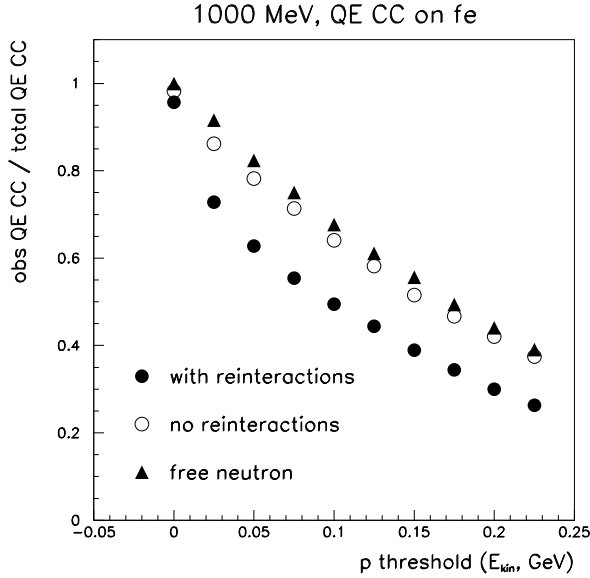


Figure 6. Acceptance for the identification of QE CC events in a fine grained detector, 1 GeV ν_μ on Fe and on free neutrons.

Positive Kaons are an excellent probe to test the Fermi distribution. They undergo only elastic and charge exchange scattering up to ≈ 800 MeV/c, and their interactions are easily modelled starting from phase shift analysis. A nice comparison of PEANUT and data on K^+Pb scattering is shown in fig. 2.

For pions, a nuclear potential has been calculated starting from the standard pion-nucleus optical potential [14].

2.4. Pion-nucleon Cross sections

Pion induced reactions are complex, mainly because of two- and three-nucleon absorption processes.

Above the pion production threshold, the inelastic interactions are handled by a resonance model.

Other pion-nucleon interactions proceed through the non-resonant channel and the p-wave channel with the formation of a Δ resonance. In nuclear matter, the Δ can either decay, resulting in elastic scattering or charge exchange, or interact with other nucleons, resulting

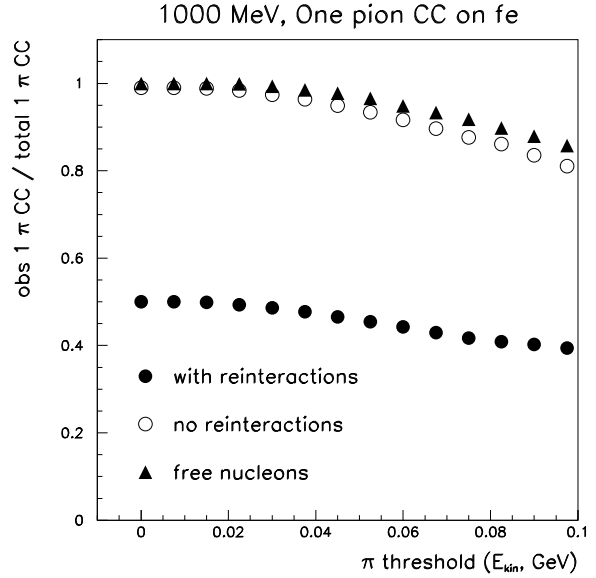


Figure 7. Acceptance for the identification of single pion CC events in a fine grained detector, 1 GeV ν_μ on Fe and on free neutrons.

in pion absorption. The width of the resonance is thus different from the free one. To account for this, the pion-nucleon total cross section used in PEANUT has been derived from the free one [15] in the following way: first, the resonant part has been extracted from the free cross section assuming for it a Breit-Wigner shape with an energy-dependent width [17]:

$$\sigma_r = \frac{8\pi}{p_{cm}^2} \frac{M_\Delta^2 \Gamma_F^2}{(s - M_\Delta^2)^2 + M_\Delta^2 \Gamma_F^2} \quad (4)$$

where p_{cm} is the pion momentum in the pion-nucleon center of mass system, s is the invariant mass squared, and $M_\Delta = 1.232$ GeV. Subtracting σ_r from the total experimental one, the non resonant scattering cross section σ_s is obtained. After that, a “new” resonant cross section σ_r^A is calculated adding to the free width Γ_F in eq. 4 the imaginary part of the (extra) width arising from nuclear medium effects. To this purpose the approach outlined in [16] has been adopted. The Δ effective width thus becomes:

$$\frac{1}{2}\Gamma_T = \frac{1}{2}\Gamma_F - Im\Sigma_\Delta \quad (5)$$

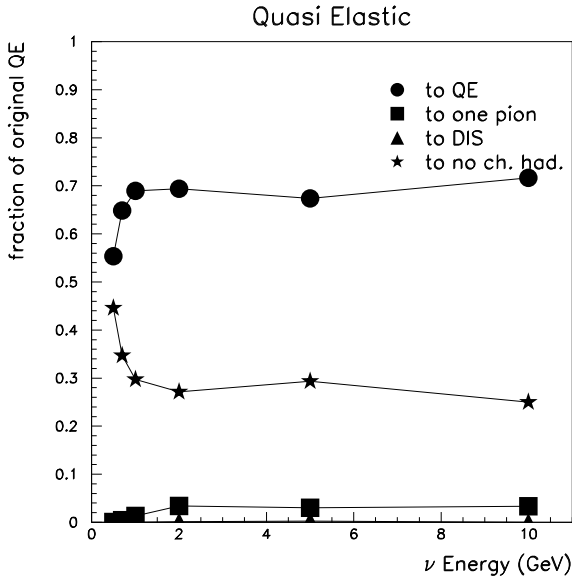


Figure 8. Fraction of generated ν_μ QE CC events that is identified as QE, single pion or DIS in a “fine grained” detector (see text), as a function of the ν energy on an Oxygen target.

$\Sigma_\Delta = \Sigma_Q + \Sigma_2 + \Sigma_3$ as calculated by Oset et.al. [16]; Σ_Q , Σ_2 and Σ_3 are the partial widths for quasielastic scattering, two body and three body absorption (see ref. [16] for details). The partial resonant cross section for each channel is obtained from σ_r^A multiplying by the ratio $\frac{\Gamma_i}{\Gamma_T}$ ($\Gamma_i = \Gamma_F$ or $2\Sigma_2$ or $2\Sigma_3$). In addition, a two-body s-wave absorption cross section has been derived from the optical model [14] as

$$\sigma_s^A(\omega) = \frac{4\pi}{p} \left(1 + \frac{\omega}{2m}\right) \text{Im}B_0(\omega)\rho \quad (6)$$

The effective in-nucleus cross section has been thus recalculated as

$$\sigma_t^A = \sigma_r^A + \sigma_s + \sigma_s^A \quad (7)$$

Isospin relations have been extensively applied both to derive the pion-nucleon cross sections in any given charge configuration from the three experimentally known, and to weight the different interaction and decay channels of the Δ resonance [17,18].

Angular distributions of reaction products are sampled according to experimental data both for

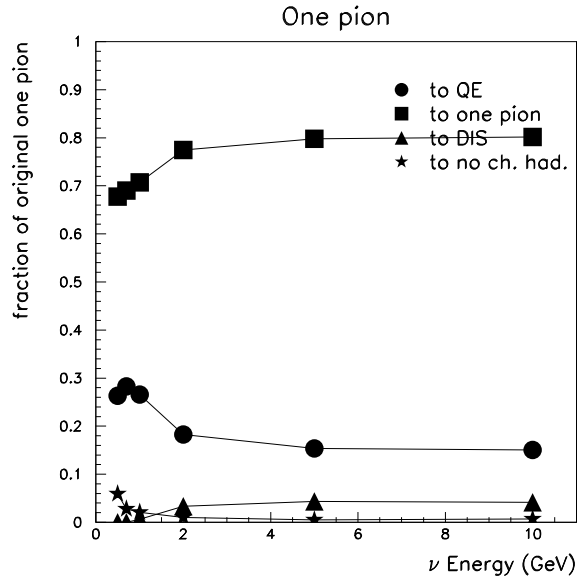


Figure 9. Fraction of generated ν_μ single pion CC events that is identified as QE, single pion or DIS in a “fine grained” detector (see text), as a function of the ν energy on an Oxygen target.

pion scattering (from free pion-nucleon) and pion absorption (from absorption on ^3He and deuterium).

The large cross section for pion absorption in the Δ region can change dramatically the kinematics of ν interactions. As an example, charged pion spectra after ν_μ interaction on Iron are shown in fig. 3, with and without the effect of pion re-interaction. For 1 GeV ν_μ energy, only 55% of the produced π escape from a Fe nucleus, and 75% from an Oxygen nucleus.

2.5. Quantistic effects

The naive use of free hadron-nucleon cross sections would lead to hadron mean free paths in nuclei by far too short with respect to reality. Indeed there are many effects that influence the in-medium cross sections, and some of them are accounted for in FLUKA .

- **Pauli blocking:** any secondary nucleon created in an intranuclear interaction must obey the Pauli exclusion principle, thus it must have enough energy to jump above the

Fermi level. For ν interactions, this results in a reduction of the cross section with respect to the free one. The effect is important at low ν energies, and is stronger for $\bar{\nu}$ due to the lower average q^2 .

- Nucleon antisymmetrization effects [19], which decrease the probability for secondary particles to reinteract on a nucleon of the same type very close to the production point
- Nucleon-nucleon hard-core correlations which also prevent secondary particles to collide again too close to the production point. Typical hard-core radii used are in the range 0.5-1 fm

2.6. Formation zone and coherence length

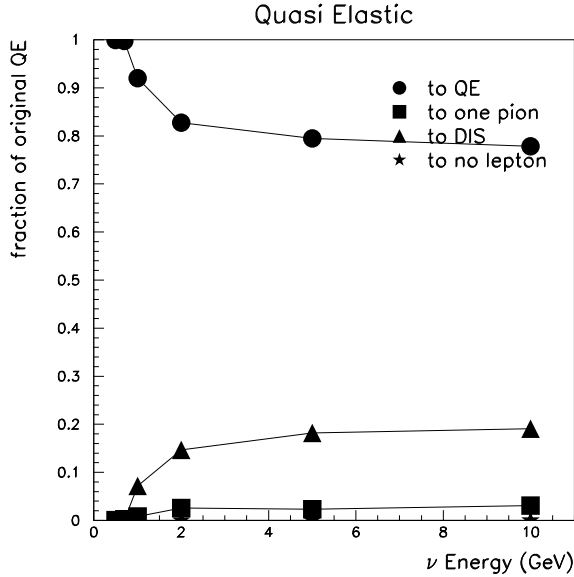


Figure 10. As fig.8 for Cerenkov cuts.

The formation zone [20] concept after pion or nucleon interactions has a privileged status among quantistic effects. It can be understood considering that hadrons are composite objects and that the typical time of strong interactions is of the order of 1 fm. If one thinks about the hadrons

emerging from an inelastic interaction, it requires some time to them to “materialize” and be able to undergo further interactions. This time interval can be expressed as

$$t_{lab} \approx \frac{\hbar E_{lab}}{p_T^2 + M^2} \quad (8)$$

This expression or, equivalently, the Stodolsky [20] one, is an approximation suitable for deep inelastic interactions, and is not fully covariant. In the FLUKA implementation, the transverse energy entering in 8 is relative to the jet axis, not to the projectile direction.

In case of elastic or quasi-elastic interactions a more rigorous approach can be followed. The “Coherence” length after (quasi)elastic or charge exchange scatterings is analogue to the formation zone concept, such interactions cannot be localized better than the position uncertainty connected with the four-momentum transfer of the collision. Reinteractions occurring at distances shorter than the coherence length would undergo interference and cannot be treated anyway as independent interactions on other nucleons. The coherence length is the analogue of the formation time concept for elastic or quasielastic interactions. It has been applied to the secondaries produced in quasielastic neutrino-nucleon interactions, with the following recipe: given a two body interaction with four-momentum transfer $q = p_{1i} - p_{1f}$, (where in our case the subscript 1 refers to the initial or final lepton, and 2 to the hadron) the energy transfer seen in a frame where the particle 2 is originally at rest is given by

$$\Delta E_2 = \nu_2 = \frac{q \cdot p_{2i}}{m_2} \quad (9)$$

From the uncertainty principle this ΔE corresponds to an indetermination in proper time given by $\Delta\tau \cdot \Delta E_2 = \hbar$, which boosted to the lab frames gives a coherence length

$$\Delta x_{lab} = \frac{p_{2lab}}{m_2} \cdot \Delta\tau = \frac{p_{2lab}}{m_2} \frac{\hbar}{\nu_2} \quad (10)$$

To illustrate the effect of the formation zone, we performed runs where the values from eqn.8 and 10 have been multiplied by arbitrary coefficients,

ranging from 0. to 100. , i.e. from no formation zone to almost no reinteractions.

- Reinteractions *increase* the hadron multiplicity with respect to the initial state kinematics, due to the buildup in the intranuclear cascade. An increase in the formation zone therefore corresponds to a suppression of the high multiplicity tail, as shown in fig 4.
- Reinteractions *populate* the hadron spectrum in the 100 MeV kinetic energy range, i.e. the *cascade* particles, and in the evaporation peak. This is well evident in fig 5. For 10 GeV ν_μ on ^{16}O , the introduction of the formation zone suppresses the cascade particles by about 40%; additional variations of a factor two have effects of the order of 15%.
- Reinteractions *depopulate* the hadron spectrum for $p > \approx 1\text{GeV}/c$. In the same test case, the decrease is around 20%. The formation zone approximately halves this percentage.
- Reinteractions *increase* the average emission angle, even for the high energy part of the spectrum. The “standard” formation zone decreases the average hadron emission angle by 10% for $p > 0.2\text{ GeV}/c$, and by 4% for $p > 2\text{ GeV}/c$ (both for 10 GeV ν_μ on ^{16}O).

3. NUCLEAR EFFECTS ON OBSERVABLES

The reconstruction of kinematic variables is affected both by nuclear effects and by instrumental effects, which are strongly detector specific. Therefore, we do not attempt here a quantitative discussion on the absolute and relative importance of these two contributions, rather we try to highlight the trends and give qualitative estimates.

To this aim, two detector “families” have been considered: water Cerenkov on one side, and “fine grained” (ICARUS-like) detectors on the other. We performed simple particle-level reconstruction, assuming perfect particle identification

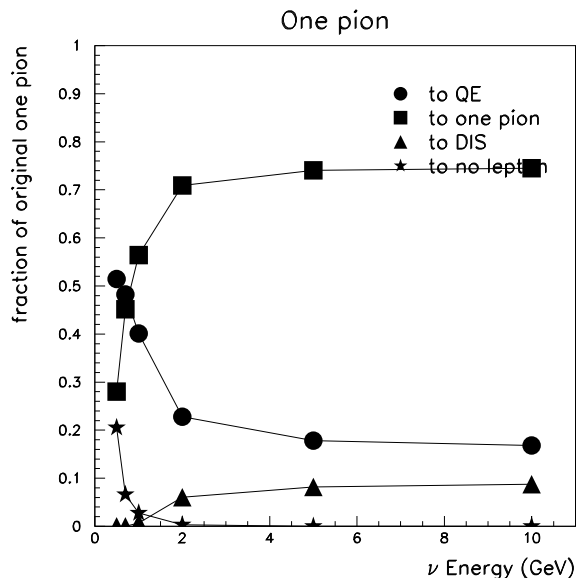


Figure 11. As fig.9 for Cerenkov cuts.

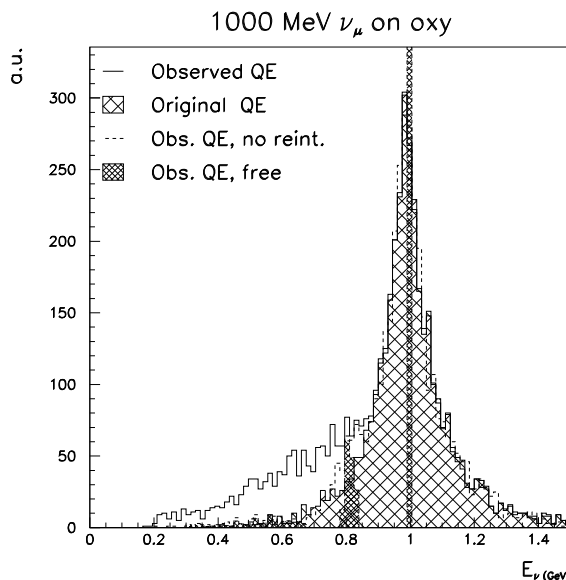


Figure 12. Reconstructed ν energy from QE CC events, for 1 GeV ν_μ on ^{16}O or free neutrons, assuming Cerenkov cuts.

above threshold, and disregarding noise, resolution, acceptance etc. For water Cerenkov, par-

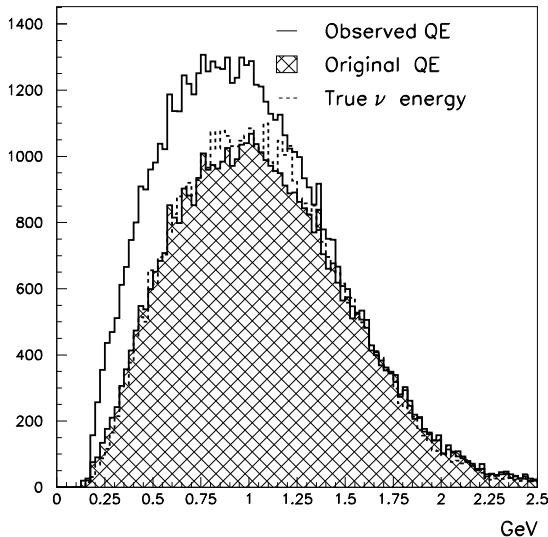


Figure 13. Reconstructed ν energy from QE CC events, for the MiniBoone ν_μ spectrum, assuming Cerenkov cuts.

ticle momentum thresholds are 5 MeV/c for e^\pm , 120 MeV/c for μ , 159 MeV/c for π^\pm , 0 for π^0 , 568 MeV/c for K^\pm , 1070 MeV/c for protons. For fine grained detectors, we tentatively assumed, in kinetic energy: 5 MeV for e^\pm , 15 MeV for μ and π^\pm , 0 for π^0 , 50 MeV for protons and K^\pm . We discarded all neutrons, heavy fragments and nuclear deexcitation photons, although in sophisticated ICARUS-like detectors part of them will be reconstructed combining imaging and calorimetric capabilities.

3.1. Channel identification

In a fine grained detector, Charged Current (CC) Quasi Elastic (QE) reactions are identified by the presence of one lepton and one proton above threshold. The acceptance of this identification depends on the experimental threshold and on nuclear effects. As shown in fig. 6, the proton threshold acts differently for bound and free target, and even in the absence of reinteractions there is a small effect due to nuclear binding. When looking at “single pion” reactions, identified as events with one lepton, and one pion above

threshold (fig 7), the effect of reinteractions becomes dramatic, around 50% of events are lost for 1 GeV ν_μ on Fe even at zero threshold, and 25% on Oxygen; it decreases slowly with increasing ν energy, reaching 40% (20%) at 10 GeV on Fe (Oxygen). These “lost” events are, however, not really lost, but only borrowed by other channels. Figs. 8 and 9 show the repartition of original QE and one-pion events in Oxygen for standard “fine grained” cuts. It can be seen that almost all the events lost in the one-pion channel populate the QE channel.

The situation is similar in the case of a water Cerenkov detector, where the QE CC are “single ring” and the single π is seen as a lepton ring plus one pion. Here the higher pion threshold increases the transfer to the QE channel (see figs. 10 and 11).

3.2. Incident ν Energy

In QE CC reactions, the incident neutrino energy E_ν can be derived from the lepton energy E_l and emission angle θ as

$$E_\nu = \frac{M \cdot E_l - 0.5 \cdot m_l^2}{M - E_l + p_l \cdot \cos(\theta)} \quad (11)$$

where M, m_l are the nucleon and lepton mass.

Fig. 12 shows the reconstructed E_ν for 1 GeV ν_μ on Oxygen, assuming water Cerenkov cuts. The red curve is obtained accepting the “original” QE events, as flagged by the generator. The spread due to the target Fermi motion is evident. Note that in FLUKA, there is no other nuclear effect on the lepton, except for Coulomb deflection. The black curve is built with the events identified as QE. The tail on the left is due to misidentified events. The red curve is again the identified QE, but with reinteractions switched off; as expected, the tail disappears, but not completely, and there is still a small bump of misidentified events. This small contribution is present also in the case of a reaction on a free nucleon (blue curve), and is due to the experimental threshold on pion detection.

In the case of a non monochromatic beam, the net effect is an enhancement of the low energy part of the reconstructed spectrum with respect to the true one, as shown in fig. 13 for the Mini-

Boone beam.

3.3. Q^2 reconstruction

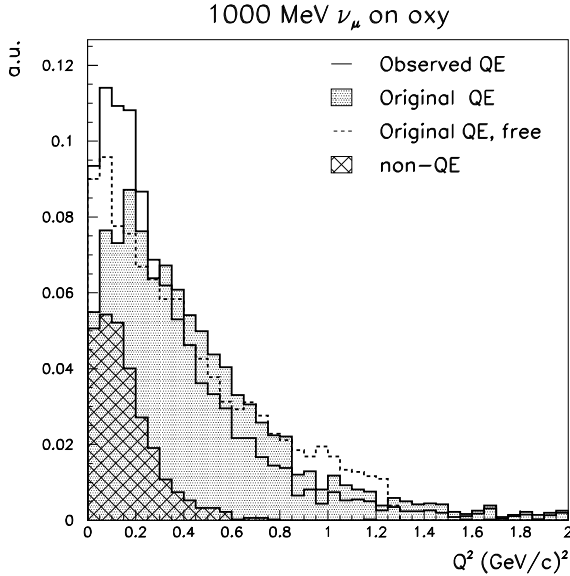


Figure 14. Reconstructed Q^2 in the QE CC interactions of 1 GeV ν_μ on ^{16}O

The analysis of K2K near detectors data show a discrepancy between the simulated and reconstructed Q^2 distributions, in particular a harder distribution in the data. We cannot perform a direct comparison without a detailed detector simulation, however we present in fig. 14 the Cerenkov-like reconstructed Q^2 distribution from 1 GeV ν_μ on Oxygen. A suppression of the low Q^2 events is evident, due to Pauli blocking. High Q^2 tails come from Fermi motion, but are partially suppressed when the proton is above threshold. The misidentified non QE events populate mainly the medium-low part. The net suppression of the low Q^2 with respect to the distribution peak is of the same order (20%) of the one observed in the K2K 1kt data.

3.4. Missing Transverse momentum

The total transverse momentum of the reaction products is a key kinematic quantity, for instance

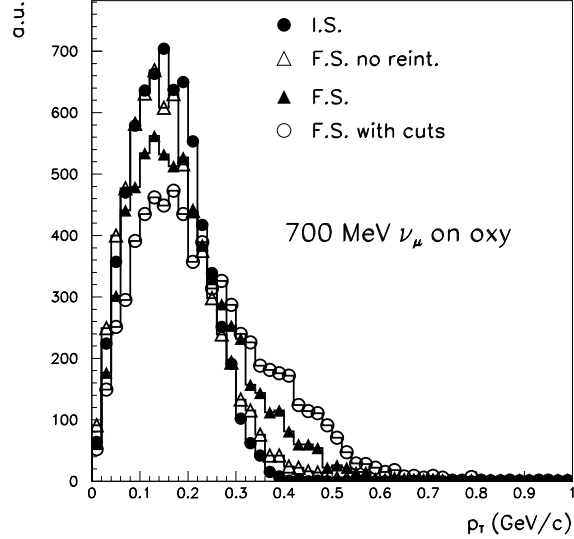


Figure 15. Total transverse momentum of reaction products, recoil nucleus excluded, for 700 MeV ν_μ CC interactions on Oxygen. “Fine grained” cuts are assumed for the black curve

for τ identification. At low ν energy (fig. 15, p_T^{miss} is dominated, already in the initial state, by the effect of Fermi motion. There is a high p_T tail due to reinteractions, that is, however, smaller than the broadening due to instrumental effects (we assume here the “fine grained” cuts, reminding again that performances better than those assumed here can be achieved). At higher energies, the reinteraction tail is more important, but the distribution can be completely masked by imprecision of event reconstruction.

3.5. Hadron Multiplicity

Hadron multiplicity is often assumed as a good probe of Monte Carlo accuracy. Indeed, as shown in fig 16, high multiplicity events are generated by reinteractions. A correct simulation of final state effects, and in particular of the formation zone, is essential to reproduce experimental data. On the other hand, experimental multiplicities and hadron spectra are an unique tool to fix the scale of the formation zone in ν interactions, that could be in principle different from the one active in

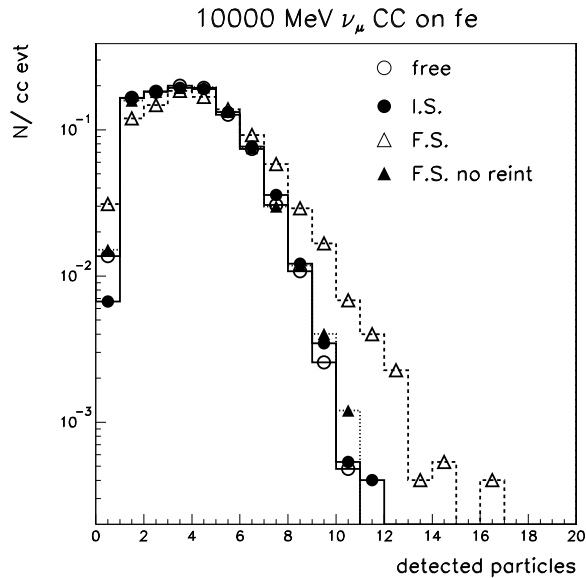


Figure 16. Charged hadron multiplicity, assuming “fine grained” cuts for 10 GeV ν_μ CC interactions on Iron

hadron-nucleus reactions.

CONCLUSIONS

The FLUKA nuclear interaction model has proven capabilities in hadron and photon induced reactions.

NUX-FLUKA has successfully simulated NOMAD data, and it is already a reliable instrument for ν -nucleus interactions. Improvements, especially for the resonant and coherent pion production mechanisms, are planned.

Nuclear effects, both on initial state and on final state, affect all kinematic quantities, but also detector specific effects are important. Therefore, the best possible detector should be used to minimize the impact of nuclear effects, and improve their understanding.

REFERENCES

1. A. Fassò, A. Ferrari, J. Ranft, and P.R. Sala, *FLUKA: Status and Prospective for Hadronic Applications*, in Proceedings of the MonteCarlo 2000 Conference, Lisbon, October

- 23–26 2000, A. Kling, F. Barão, M. Nakagawa, L. Távora, P. Vaz eds., Springer-Verlag Berlin, 955 (2001); A. Ferrari, and P.R. Sala, *The Physics of High Energy Reactions*, in Proceedings of Workshop on Nuclear Reaction Data and Nuclear Reactors Physics, Design and Safety, A. Gandini, G. Reffo eds., Trieste, Italy, April 1996, **2**, 424 (1998).
2. A. Rubbia “NUX- neutrino generator”, 1st Workshop on Neutrino - Nucleus Interactions in the Few GeV Region (NuInt01), Tsukuba, Japan, 13-16 Dec 2001, neutrino.kek.jp/nuint01/slide/Rubbia.1.pdf
3. E. Gadioli, and P.E. Hodgson, *Pre-equilibrium Nuclear Reactions*, Clarendon Press, Oxford, (1992).
4. J. J. Griffin, Phys. Rev. Lett., **17**, 438 (1966).
5. V.F. Weisskopf, Phys. Rev., **52**, 295 (1937).
6. E. Fermi, Prog. Theor. Phys., **5**, 1570 (1950).
7. M. Epherre and E. Gradsztajn, J. Physique, **18**, 48 (1967).
8. A. Ferrari, P.R. Sala, J. Ranft, and S. Roesler, Z. Phys., **C71**, 75 (1996).
9. M.E. Gyropeos, G.A. Lalazissis, S.E. Massen and C.P. Panos, J. Phys., **G17**, 1093 (1991).
10. L.R.B. Elton, *Nuclear Sizes*, Oxford University Press, Oxford (1961).
11. W.D. Myers, Nucl. Phys., **A204**, 465 (1973).
12. W.D. Myers, *Droplet Model of Atomic Nuclei*, IFI/Plenum Data Company, New York (1977).
13. C.M. Kormanyos et al., Phys. Rev., **C51**, 669 (1995).
14. T. Ericson and W. Weise, *Pions and Nuclei*, Clarendon Press, Oxford, (1988).
15. Phase shift solutions KH78, KH80, in *Landolt-Börnstein, new series*, **Vol. 9, part II**, Springer-Verlag, (1983).
16. E. Oset, and L.L. Salcedo, Nucl. Phys., **A468**, 631 (1987).
17. J.N. Ginocchio, Phys. Rev., **C17**, 195 (1978).
18. M.J. Vicente Vacas, and E. Oset, Nucl. Phys., **A568**, 855 (1994).
19. A. Bohr, B.R. Mottelson, *Nuclear Structure*, **Vol. 1**, W.A. Benjamin, Inc. (1969).
20. L. Stodolski, Proc. of the *Vth Intern. Coll. on Multiparticle Reactions*, Oxford, 577 (1975).